Stress-induced R-M_{A}-M_{C}-T symmetry changes in BiFeO_{3} films

H. M. Christen, J. H. Nam, H. S. Kim, A. J. Hatt, and N. A. Spaldin

Phys. Rev. B **83**, 144107 — Published 14 April 2011

DOI: 10.1103/PhysRevB.83.144107

Stress-induced R-M_A-M_C-T symmetry changes in $BiFeO_3$ films

H.M. Christen,[1] J.H. Nam[1,2], H.S. Kim[1,3], A. J. Hatt[4,5], and N. A. Spaldin[4,6]

[1]Materials Science and Technology Division, Oak Ridge National Laboratory, Oak Ridge, TN 37831, USA

[2]Optic and Electronic Ceramics Division, Korea Institute of Ceramic Engineering and Technology (KICET), Seoul 153-801, Republic of Korea

[3]Department of Physics, University of Warwick, Coventry CV4 7AL UK.

[4]Materials Department, University of California, Santa Barbara, CA 93106, USA

[5]Molecular Foundry, Lawrence Berkeley National Laboratory, Berkeley CA 94720, USA

[6]Department of Materials, ETH Zurich, CH-8093 Zürich, Switzerland

PACS 77.80.bn; 77.55Nv; 77.80.Jk; 68.55.aj;

ABSTRACT

Recent reports on epitaxial $BiFeO_3$ films show that the crystal structure changes from nearly rhombohedral ("R-like") to nearly tetragonal ("T-like") at strains exceeding ≈-4.5%, with the "T-like" structure being characterized by a highly-enhanced *c/a* ratio. While both the "R-like" and the "T-like" phases are monoclinic, our detailed x-ray diffraction results reveal a symmetry change from M_A and M_C type, respectively, at this "R-like"-to-"T-like" transition. Therefore, the ferroelectric polarization is confined to different (pseudocubic) planes in the two phases. By applying additional strain or by modifying the unit cell volume of the film by substituting Ba for Bi, the monoclinic distortion in the "T-like" M_C phase is reduced, i.e. the system approaches a true tetragonal symmetry. Therefore, in going from bulk to highly-strained films, a phase sequence of rhombohedral(R)-to-monoclinic("R-like" M_A)-to-monoclinic("T-like" M_C)-to-tetragonal(T) is observed. This sequence is otherwise seen only near morphotropic phase boundaries in lead-based solid-solution perovskites (i.e. near a compositionally induced phase instability), where it can be controlled by electric field, temperature, or composition. Our results now show that this evolution can occur in a lead-free, stoichiometric material and can be induced by stress alone.

I. INTRODUCTION

The recent discovery of a stress-induced structural phase transition in the single-component perovskite $BiFeO_3$ (refs 1-3) has revived interest in this lead-free ferroelectric and points to new applications of a material already being the most promising multiferroic[4]. The coexistence of different phases may lead to large piezoelectric coefficients[3], a property that is typically associated with complex solid solutions of lead-based perovskites. In this work, we report combined experimental and computational results showing that the stress-induced phase transitions in $BiFeO_3$ follow the path of rhombohedral(R)-to-monoclinic(M_A)-to-monoclinic(M_C)-to-tetragonal(T), where both M_C and T show highly enhanced *c/a* ratios of out-of-plane (*c*) to in-plane (*a*) lattice parameters. Specifically, our detailed results shed attitional light onto a very recent report of a symmetry change at the "R-like"-to-"T-like" transition, accompanied by a change of orientation of the ferroelectric polarization[5]. Here we show that this symmetry change is part of a complete R-M_A-M_C-T sequence that is otherwise observed only near morphotropic phase boundaries (MPBs) in lead-based perovskites (i.e. near a compositionally induced phase instability), where it is controlled by electric field, temperature, or composition (refs 6-8). Our results represent the first time that the full R-M_A-M_C-T evolution has been induced in a single component system using strain alone, and show that substrate-imposed symmetry lowering results in a similar phase instability as the proximity to a MPB in solid solutions.

Epitaxial films provide an ideal platform to study the effect of biaxial stress on complex materials. When the rhombohedral perovskite $BiFeO_3$ is grown on a substrate having a square in-plane lattice, its symmetry is lowered to monoclinic, except in free-standing membranes and very

thick films that remain rhombohedral. At tensile to moderate-compressive strains, the monoclinic structure loosely resembles that of the rhombohedral bulk, and we refer to it as the "R-like" phase. Compressive strains exceeding about -4.5% result in a strongly increased out-of-plane lattice parameter c_{pc}, leading to a c_{pc}/a_{pc} ratio of about 1.25 (where a_{pc} is the in-plane lattice parameter and the subscript *pc* refers to the pseudo-cubic notation) and an abrupt change in Fe coordination. This monoclinic phase thus resembles that of a super-tetragonal perovskite, and we therefore refer to it as "T-like".

Both "R-like" and "T-like" phases are ferroelectric. The polarization ***P*** points approximately along the $[111]_{pc}$ direction in the "R-like" phase[9,11] and rotates towards the $[001]_{pc}$ direction with increasing compressive strain. For the "T-like" phase, the very large values of the measured projection of ***P*** onto the $[001]_{pc}$ direction[1,2] agree with theoretical predictions of a polarization predominantly along $[001]_{pc}$ (ref 10), although surprisingly there is a report of a strong in-plane component using piezoresponse force microscopy[12].

The transition between the two monoclinic "R-like" and "T-like" phases has been labeled *iso-symmetric*; in this work we show that this is an oversimplification and in fact the evolution with increasing strain is from an "R-like" monoclinic M_A phase of *Cc* or *Cm* symmetry to a "T-like" monoclinic M_C phase of *Pc* or *Pm* symmetry with increasing strain, in agreement with a recent report of results from x-ray diffraction, piezoresponse force microscopy, and phenomenological modeling[5]. Then at very high strain values, which have not yet been accessed through direct coherent heteroepitaxy alone, a fully tetragonal *P4mm* phase is obtained.

II. EXPERIMENTAL AND COMPUTATIONAL METHODS

Epitaxial films were grown by pulsed-laser deposition at a substrate temperature of 700°C, a background pressure of 25 - 50 mTorr, using a KrF excimer laser (wavelength 248 nm, energy per pulse 550 - 590 mJ, pulse repetition rate 5 Hz) and sintered targets containing a 10% excess of Bi. At the target-to-substrate distance of 50 mm, the resulting deposition rate was ~0.2 Å/pulse. Solid-solution films ($Bi_{1-x}Ba_xFeO_3$) were obtained by a method in which submonolayer amounts of $BiFeO_3$ and $BaFeO_3$ are sequentially and repeatedly deposited by ablating from two separate targets[13]. All samples were then characterized using a PANalytical X'Pert Pro 4-circle x-ray diffractometer using Cu Kα radiation. Reciprocal space maps (RSMs) were recorded by a sequence of θ-2θ scans at different ω offsets, and are shown in plots of intensity as a function of q in reciprocal lattice units (rlu), where $q = \pi/4d$.

First principles calculations were carried out using density functional theory as implemented in the Vienna Ab-initio Simulation Package, employing the PAW method and the local spin density approximation (LSDA) plus a Hubbard U term on the Fe d states, as described elsewhere[11]. We achieve well-converged total energies using a 500 eV plane-wave cutoff and a 4x4x4 k-point grid. Space group determination was performed with the software FINDSYM [14].

III. STRUCTURAL ANALYSIS: M_A-to-M_C TRANSITION

First we describe the structures of the relevant phases. Consistent with all literature and current experimental and computational results we take $\beta \neq 90°$ to be between the a and c axes. Since

only four monoclinic space groups (*Pm, Pc, Cm*, and *Cc*) can show a non-vanishing polarization in the *c* direction, we restrict our discussion to the corresponding primitive (*P*) or base-centered (*C*) unit cells containing either a mirror (*m*) or glide (*c*) plane perpendicular to the *b* axis; ***P*** is then constrained by symmetry to its mirror or glide plane, ***P*** || [*u0v*]. We use standard notation[15] to distinguish three monoclinic cases based on the orientation of ***P*** with respect to the pseudocubic coordinates: M_A and M_B for ***P*** || $[uuv]_{pc}$, with $u<v$ and $u>v$, respectively; and M_C for ***P*** || $[u0v]_{pc}$. (The tetragonal (T), rhombohedral (R), and orthorhombic (O) phases correspond to a constraint of ***P*** to a *symmetry axis* along $[001]_{pc}$, $[111]_{pc}$, or $[011]_{pc}$, respectively, see Fig. 1a).

M_A and M_B both correspond to either *Cm* or *Cc* space groups, with a monoclinic unit cell rotated by 45° with respect to the pseudocubic structure (i.e. [*u0v*] || $[uuv]_{pc}$), and are obtained by shearing the cubic perovskite cell along the $[110]_{pc}$ direction (Fig. 1b). For simplicity we restrict our discussion to M_A. In contrast, M_C corresponds to either *Pm* or *Pc*, resulting from a shear along $[100]_{pc}$. In Figs. 1b and c we sketch the smallest M_A and M_C unit cells that are also compatible with common types of antiferromagnetism and octahedral tilt patterns[16]. This requires a $\sqrt{2}$ x $\sqrt{2}$ x 2 supercell for the (centered) M_A and a 2 x 2 x 2 supercell for the (primitive) M_C phase.

We study the structure of $BiFeO_3$ at different compressive biaxial strains in epitaxial films on $SrTiO_3$ (001), $LaAlO_3$ $(001)_{pc}$ and $YAlO_3$ $(001)_{pc}$ substrates. All samples are epitaxial and free of impurity phases, with only the $(00l)_{pc}$ peaks detected in normal θ-2θ x-ray diffraction (XRD) scans, see Fig. 2. 270 nm thick films on $SrTiO_3$ substrates show a c_{pc}-axis lattice parameter of 3.99Å, corresponding to the "R-like" phase, as in our previous work[9], while for those on $LaAlO_3$

we determine c_{pc} = 4.64Å, i.e. we find the "T-like"-phase (again in films with a thickness of 270 nm). Growth of monoclinic $BiFeO_3$ on a higher-symmetry substrate requires the formation of a multi-domain structure. We observe single peaks in the ω-scans (rocking curves) through the $(00l)_{pc}$ film positions (data not shown) showing that the $(00l)_{pc}$ planes of all domains are parallel to each other, as also reported elsewhere[17-19]. Reciprocal space maps (RSMs) through the $\{113\}_{pc}$ and the $\{103\}_{pc}$ family of peaks are shown in Fig. 3a. The observation of a two-fold and three-fold splitting along the $[113]_{pc}$ and the $[103]_{pc}$ directions, respectively, indicates the type of monoclinic distortions. In fact, as illustrated in Fig. 1d, it is easily seen that the monoclinic family of peaks splits three-fold for $\{hhl\}$ and two-fold for $\{h0l\}$ (refs 20-22). With the 45° rotation of a with respect to a_{pc} in the M_A monoclinic structure but $a \parallel a_{pc}$ in M_C, the RSMs for the two monoclinic structures look distinctively different. Clearly, our results for "T-like"-$BiFeO_3/LaAlO_3$ are consistent only with the M_C structure, and thus distinctively different from that in "R-like"-$BiFeO_3$, for which our data shown below and that of a number of authors[9,17-22] clearly indicate the M_A structure.

The M_C symmetry of the "T-like" phase is confirmed in in-plane (grazing-incidence) XRD scans through the substrate's 110_{pc} and 100_{pc} peaks (Fig. 3b), which shows a single peak along the pseudocubic face diagonal, but a split peak along 100_{pc}. From a refinement of 20 diffraction peaks combined with relative (peak separation) measurements from these RSMs and in-plane scans we find for "T-like"-$BiFeO_3$ a = 2 x 3.84(2) Å, b = 2 x 3.70(2) Å, c = 2 x 4.64(2) Å, and β = 87.9(2)° (where the doubling of the unit cell is not seen in the data but considered for compatibility with antiferromagnetism and octahedral tilts). Thus, these data conclusively show that monoclinic "T-like"-$BiFeO_3$ exhibits a M_C structure belonging to either the *Pm* or *Pc* space

groups. Note that Raman data[12], while originally interpreted in terms of *Cc*, are insufficient to determine the type of monoclinic distortion. However, earlier x-ray data presented but not fully analyzed by Iliev *et al.*[23], supplemental data in Ref. 3, as well as the more recent results mentioned above[5] are all fully consistent with our observations.

IV. COMPUTATIONAL RESULTS

Previous first principles calculations found the M_A (*Cc*) structure to be the ground state for "T-like"-$BiFeO_3$ (ref 11) but an exhaustive search of all possible monoclinic shear orientations, polarization orientations, c/b ratios and monoclinic angles, was not previously performed. Therefore, here we make such a search, looking explicitly for the M_C phase, and using a 2 x 2 x 2, 40 atom unit cell that accommodates the distortions expected for the M_C phase. We find that G-type antiferromagnetic order is energetically indistinguishable from C-type for a few representative structures, and hereafter maintain G-type for all calculations.

To most closely simulate the experimental conditions, we constrain the in-plane lattice parameters to the measured values scaled by the ratio of experimental to local spin density approximation (LSDA) values of the bulk lattice parameter, (giving $b = 2 \times 3.69$ Å), and we use the experimental $c/b = 1.25$. We then search for the lowest energy structure for shear orientations along $[110]_{pc}$ and $[100]_{pc}$, corresponding to M_A and M_C, respectively, relaxing β and a/b for each. In our search for the ground state, we initialize the system to a number of likely polarization orientations and patterns of octahedral rotations to explore the structural phase space as completely as possible within the computational time limitations.

We find three phases that are very close in energy: the M_A (*Cc*) phase studied in previous work remains lowest in energy[11], but we also identify two low energy metastable phases with shear along $[100]_{pc}$ corresponding to space groups *P1* and *Pm*. Figure 4 shows the total calculated energy per formula unit as a function of the shear angle β for these three phases, and Table I summarizes the results. As before, the M_A (*Cc*) phase has $a^-b^-c^0$ rotations and a polar displacement along the glide plane; in contrast, the M_C (*Pm*) phase has $a^-b^0c^0$ rotations and a polar displacement along the mirror plane. The triclinic *P1* phase has $a^-b^-c^0$ rotations but a polar displacement with components along all three lattice directions. Note that a continuous transition from M_A to M_C would require an intermediate phase (dashed arrow in Fig. 1a)[15,24], such as this *P1* structure. The energies of the metastable M_C (*Pm*) and the *P1* phases are higher in energy than the M_A phase by only ~4 meV per formula unit. In comparison, restricting the *c/a* ratio to a value corresponding simply to an elastic deformation of the "R-like" structure rather than allowing a transition to the "T-like" phase would result in an energy that is more than 100 meV higher[11]. Other possible phases that have been considered in the literature, such as the Cm (ref 25) and tetragonal P4mm are considerably higher in energy (~15 and ~20 meV per formula unit respectively). The energetic proximity of the M_A (*Cc*), M_C (*Pm*), and *P1* phases is consistent with recent DFT calculations predicting a remarkably flat energy landscape between various polymorphs of $BiFeO_3$.[26] These authors also report that the calculated energy differences are highly sensitive to the choice of pseudopotential, but that LSDA+U gives the most reliable agreement with experiment for strained $BiFeO_3$.[26] Note that previously calculated domain wall energies in R-$BiFeO_3$ (~100 meV per unit cell)[27] are also two orders of magnitude larger than the energy differences between these various "T-like" phases, suggesting that factors such as the

ability to form favorable domain patterns might be more important than absolute total energies of different phases in determining the ground state structure adopted by a strained film.

Next we explore whether at higher strain values the monoclinicity can be completely removed and a genuine tetragonal phase can be formed. When we impose in our calculations an exceedingly large in plane strain of 10% ($a = b = 2$ x 3.5 Å) we indeed find a tetragonal (*P4mm*) ground state with $c / a = 1.41$ and the octahedral rotations reduced to zero.

V. INCREASED TETRAGONALITY BY STRAIN AND Ba-SUBSTITUTION

To verify the computational prediction of a *P4mm* phase experimentally we first grew films on orthorhombic (110)-oriented $YAlO_3$ substrates, having a pseudocubic in-plane lattice parameter of 3.704 Å (ref 28), i.e. significantly smaller than that of $LaAlO_3$. Normal θ-2θ x-ray scans (Fig. 2) show that the $BiFeO_3$ separates both into the "R-like" and "T-like" phases. Nevertheless, the peaks corresponding to the "T-like"-phase can again be indexed as M_C, but with $a = 2$ x 3.82(4) Å, $b = 2$ x 3.72(4) Å, $c = 2$ x 4.66(2) Å, and $\beta = 88.5(3)°$. Therefore, the M_C symmetry is preserved but the structure becomes closer to tetragonal under additional stress, with *b/a* closer to unity and β closer to 90°. The RSMs for this sample are shown in Figure 5 a and b.

To induce a larger effective strain, we next modify our "T-like" $BiFeO_3$ via the substitution of Ba for Bi to make a $Bi_{1-x}Ba_xFeO_{3-\delta}$ solid-solution with $\delta \approx x/2$ (ref 28). As we have shown previously[28], this substitution results in an enlarged unit cell volume – as a consequence of both the larger ionic radius of Ba^{2+} and the formation of oxygen vacancies – and therefore a larger

effective biaxial compressive stress when grown on a same substrate. In Fig. 5e-g, we show RSMs through the {226} family $x = 0$, 0.02, and 0.08. A clear transition from the monoclinic (M_C) to a tetragonal structure is observed, with no measurable peak splitting in either {226} or {206} (Fig. 5 g,h) at $x = 0.08$. Figure 5c and d show the evolution of β and the ratio of the in-plane lattice parameters, *b/a*, as a function of Ba content, showing the gradual transition from the monoclinic to the tetragonal structure.

While the stabilization of this true tetragonal structure is not purely due to epitaxial strain, in combination with the data for $BiFeO_3$ on $YAlO_3$ and the computational results, it implies that additional biaxial stress applied to the M_C structure will result in a true tetragonal phase. Therefore, $BiFeO_3$ can undergo the complete R-M_A-M_C-T path of transitions. This is best summarized by comparing RSMs for four different samples (see Fig. 6), corresponding each to a different symmetry. The 2 μm thick $BiFeO_3$ film on $SrTiO_3$ (bottom panel) is essentially relaxed due to its large thickness, and shows a diffraction pattern similar to that found for rhombohedral $BiFeO_3$ elsewhere[10,29]. A thinner film of $BiFeO_3$ shows the typical diffraction pattern for "R-like" $BiFeO_3$ with the M_A structure as discussed elsewhere[9,17-22]. For the "T-like" $BiFeO_3$ sample (M_C structure) and the $Bi_{0.92}Ba_{0.08}FeO_3$ (T) the data in Fig. 6 are taken from Figs. 3 and 5, respectively.

Symmetry changes as a consequence of external parameters have been observed in $BiFeO_3$ in a number of experiments. For example, films on $SrTiO_3$ show a transition near 750°C from M_A to M_C with temperature[31], presumed to be associated with the ferroelectric-to-paraelectric phase transition. Isostatic pressure applied to powders results in a transition from *R3c* to a non-ferroelectric *C2/m* monoclinic phase[32]. Computational results indicate a broad variety of phase

changes with electric field[33]. However, the changes observed here are most similar in nature to those observed in the lead-based relaxor ferroelectrics (1-x)Pb($Mg_{1/3}Nb_{2/3}$)O_3 – x($PbTiO_3$) (PMN-PT) and (1-x)Pb($Zn_{1/3}Nb_{2/3}$)O_3 – x($PbTiO_3$) (PZN-PT). In fact, synchrotron x-ray diffraction data[6] on PZN-PT lead to a (field, composition)-phase diagram in which the R-M_A-M_C-T path can be traversed either in the field or composition direction. Similarly, the R-M_A-M_C-T path is also seen in the (field, temperature)-phase diagram of PMN-PT (refs 7-8) and PZN-PT (ref 8). These last results further suggest the possibility of similar but stress-induced structural changes, but there has been no experimental observation thereof. Intriguingly, calculations for Pb($Zr_{1-x}Ti_x$)O_3 indicate the presence of a triclinic phase when the path from M_A to M_C is traversed via application of an electric field[24] or changes in composition[15]. Our computational results for $BiFeO_3$ show the energetic proximity of the M_C and a triclinic (*P1*) phase and thus further illustrate the analogies between this single-component perovskite and the lead-oxide solid solutions.

VI. CONCLUSIONS

The results presented here clarify that the "R-like"-to-"T-like" transition in $BiFeO_3$ is not as previously thought "iso-symmetric" but part of a broader R-M_A-M_C-T path in which the polarization orientation changes from one lying within the $(1\,\bar{1}\,0)_{pc}$ plane to one in the $(010)_{pc}$ plane. The observation of this R-M_A-M_C-T phase sequence in a stoichiometric compound, rather than in a solid-solution near a MPB, allows us to draw important conclusions regarding the control of structural and ferroelectric phase transformations and the potential of achieving technologically important piezoelectric properties in lead-free materials. In the lead-oxide solid

solutions, the stability of the monoclinic phases is limited to a narrow region in composition space near the MPB. Given the delicate energy balance between the involved phases and possible local variations in stoichiometry, open questions remain in these solid solutions regarding the origins of these phase transitions and the mechanisms that can be used to control them (see ref 34 for a recent review). Our experimental and computational observations on $BiFeO_3$ now show that a stoichiometric material can mimic the behavior of a solid-solution near its MPB, illustrate the strong effect of substrate-induced symmetry lowering, and demonstrate that the R-M_A-M_C-T path can be controlled by epitaxial strain alone. Computationally, we find that the M_C phase is very close but not lower in energy than other similar structures. This may indicate the importance of the possible domain patterns and domain wall energies on the actual crystal structure, as such effects are not considered in our calculations. Our results thus show shows that "strain engineering" is an important tool both in fundamental studies to understand complex phase equilibria as well as in approaches to find new, lead-free materials with technologically relevant properties, such as large piezoelectric coefficients.

ACKNOWLEDGEMENTS

H.S.K and H.M.C acknowledge support from the Laboratory Directed Research and Development Program of Oak Ridge National Laboratory, managed by UT-Battelle, LLC, for the U. S. Department of Energy. J.H.N. was supported by the Republic of Korea, Ministry of Knowledge and Economy, Visiting Scientists Program, under IAN: 16B642601, with the U.S. Department of Energy. NAS and AJF were supported by NSF Awards No. DMR-0820404 and No. NIRT-0609377. Computational resources used include the SGI Altix Cobalt system and the

TeraGrid Linux Cluster Mercury at the National Center for Supercomputing Applications under Grant No. DMR-0940420 and CNSI Computer Facilities at UC Santa Barbara under NSF Grant No. CHE-0321368

REFERENCES

1. D. Ricinschi, K.-Y. Yun, and M. Okuyama, J. Phys.: Condens. Matter **18**, L97 (2006).
2. H. Béa, B. Dupé, S. Fusil, R. Mattana, E. Jacquet, B. Warot-Fonrose, F. Wilhelm, A. Rogalev, S. Petit, V. Cros, A. Anane, F. Petroff, K. Bouzehouane, G. Geneste, B. Dkhil, S. Lisenkov, I. Ponomareva, L. Bellaiche, M. Bibes, and A. Barthélémy, Phys. Rev. Lett. **102**, 217603 (2009).
3. R. J. Zeches, M. D. Rossell, J. X. Zhang, A. J. Hatt, Q. He, C.-H. Yang, A. Kumar, C. H. Wang, A. Melville, C. Adamo, G. Sheng, Y.-H. Chu, J. F. Ihlefeld, R. Erni, C. Ederer, V. Gopalan, L. Q. Chen, D. G. Schlom, N. A. Spaldin, L. W. Martin, and R. Ramesh, Science **326**, 977 (2009).
4. J. Wang, J. B. Neaton, H. Zheng, V. Nagarajan, S. B. Ogale, B. Liu, D. Viehland, V. Vaithyanathan, D. G. Schlom, U. V. Waghmare, N. A. Spaldin, K. M. Rabe, M. Wuttig, and R. Ramesh, Science **299**, 1719 (2003).
5. Z. Chen, Z. Luo, C. Huang, Y. Qi, P. Yang, L. You, C. Hu, T. Wu, J. Wang, C. Gao, T. Sritharan, and L. Chen, Adv. Funct. Mater. **21**, 133 (2010).
6. B. Noheda, Z. Zhong, D. E. Cox, G. Shirane, S-E. Park, and P. Rehrig, Phys. Rev. B **65**, 224101 (2002).
7. F. Bai, N. Wang, J. Li, D. Viehland, P. M. Gehring, G. Xu, and G. Shirane, J. Appl. Phys. **96**, 1620 (2004).
8. M. Davis, D. Damjanovic, and N. Setter, Phys. Rev. B **73**, 014115 (2006).
9. D. H. Kim, H. N. Lee, M. D. Biegalski, and H. M. Christen, Appl. Phys. Lett. **92**, 012911 (2008).

10. H. W. Jang, S. H. Baek, D. Ortiz, C. M. Folkman, R. R. Das, Y.-H. Chu, P. Shafer, J. X. Zhang, S. Choudhury, V. Vaithyanathan, Y. B. Chen, D. A. Felker, M. D. Biegalski, M. S. Rzchowski, X. Q. Pan, D. G. Schlom, L. Q. Chen, R. Ramesh, and C. B. Eom, Phys. Rev. Lett. **101**, 107602 (2008).
11. A. J. Hatt, N. A. Spaldin, and C. Ederer, Phys. Rev. B **81**, 054109 (2010).
12. D. Mazumdar, V. Shelke, M. Iliev, S. Jesse, A. Kumar, S. V. Kalinin, A. P. Baddorf, and A. Gupta, Nano Lett. **10**, 2555 (2010).
13. H. M. Christen and G. Eres, G. J. Phys.: Condens.Matter **20**, 264005 (2008).
14. H. T. Stokes and D. M. Hatch. J. Appl. Crystallogr. **38**, 237 (2005); H. T. Stokes H. T. and D. M. Hatch (2007). ISOTROPY, stokes.byu.edu/isotropy.html.
15. D. Vanderbilt and M. H. Cohen, Phys. Rev. B **63**, 094108 (2001).
16. A. M. Glazer, Acta Cryst. **B28**, 3384 (1972).
17. X. Qi, M. Wei, Y. Lin, Q. Jia, D. Zhi, J. Dho, M. G. Blamire, and J. L. MacManus-Driscoll, Appl. Phys. Lett. **86**, 071913 (2005).
18. C. J. M. Daumont, S. Farokhipoor, A. Ferri, J. C. Wojdel, J. Iniguez, B. J. Kooi, and B. Noheda, Phys. Rev. B **81**, 144115 (2010).
19. H. Liu, P. Yang, K. Yao, and J. Wang, Appl. Phys. Lett. **96**, 012901 (2010).
20. K. Saito, A. Ulyanenkov, V. Grossmann, H. Ress, L. Bruegemann, H. Ohta, T. Kurosawa, S. Ueki, and H. Funakubo, Jpn. J. Appl. Phys. **45**, 7311 (2006).
21. G. Xu, H. Hiraka, G. Shirane, J. Li, J. Wang, and D. Viehland, Appl. Phys. Lett. **86,** 182905 (2005).

22. M. B. Holcomb, L. W. Martin, A. Scholl, Q. He, P. Yu, C.-H. Yang, S. Y. Yang, P.-A. Glans, M. Valvidares, M. Huijben, J. B. Kortright, J. Guo, Y.-H. Chu, and R. Ramesh, Phys. Rev. B **81**, 134406 (2010).
23. M. N. Iliev, M. V. Abrashev, D. Mazumdar, V. Shelke, and A. Gupta, Phys. Rev. B **82**, 014107 (2010).
24. L. Bellaiche, A. García, and D. Vanderbilt, Phys. Rev. B **64**, 060103 (2001).
25. B. Dupé, I. C. Infante, G. Geneste, P.-E. Janolin, M. Bibes, A. Barthélémy, S. Lisenkov, L. Bellaiche, S. Ravy, and B. Dkhil, Phys. Rev. B **81**, 144128 (2010).
26. O. Diéguez, O.E. González-Vázquez, Jacek C. Wojdeł, and J. Íñiguez, arXiv:1011.0563v2
27. A. Lubk, S. Gemming , and N. A. Spaldin. Phys. Rev. B **80**, 104110 (2009).
28. N. L. Ross, J. Zhao, and R. J. Angel. J. Solid State Chem. **177**, 1276 (2004).
29. C. J.C. Bennett, H.S. Kim, M. Varela, M. D. Biegalski, D.H. Kim, D. P. Norton, H.M. Meyer III, and H. M. Christen. Submitted.
30. D. S. Rana, K. Takahashi, K. R. Mavani, I. Kawayama, H. Murakami, M. Tonouchi, T. Yanagida, H. Tanaka, and T. Kawai, Phys. Rev. B **75**, 060405 (2007).
31. H. Toupet, F. Le Marrec, C. Lichtensteiger, B. Dkhil, and M. G. Karkut, Phys. Rev. B **81**, 140101 (2010).
32. R. Haumont, P. Bouvier, A. Pashkin, K. Rabia, S. Frank, B. Dkhil, W. A. Crichton, C. A. Kuntscher, and J. Kreisel, Phys. Rev. B **79**, 184110 (2009).
33. S. Lisenkov, D. Rahmedov, and L. Bellaiche, Phys. Rev. Lett. **103**, 047204 (2009).
34. B. Noheda and D. E. Cox. Phase Transitions **79**, 5 (2006).

FIGURE CAPTIONS

Figure 1. Schematic comparison of monoclinic structures. **a**: polarization direction in differently distorted perovskite structures: the polarization points in a direction parallel to that connecting the origin with the indicated dots for R, O, and T, or with any point on the lines labeled M_A, M_B, and M_C. The path R – M_A – M_C – T observed here and in relaxor ferroelectrics is indicated by arrows (see text). **b** and **c**: Smallest unit cells (with appropriate antiferromagnetic order and octahedral tilt patterns) for the two possible monoclinic structures, each resulting from a shear distortion in the direction of the indicated arrow. Thin lines indicate the primitive perovskite unit cell. M_A is a centered unit cell belonging to space group *Cc* or *Cm*, M_C is a primitive unit cell, space group *Pc* or *Pm*. **d**: Schematic representation of reciprocal space maps of a monoclinic structure, indexed in the monoclinic system and the pseudocubic notation for M_A and M_B, respectively.

Figure 2. (color online) Comparison of $BiFeO_3$ (BFO) films grown on different substrates. The semi-logarithmic plot shows results from X-ray θ-2θ scans for four BFO films of different thickness and on different substrates (offset vertically for clarity): $SrTiO_3$ (STO), $LaAlO_3$ (LAO), and $YAlO_3$ (YAO). The 002_{pc} peaks for the film and substrates are shown. Films on $SrTiO_3$ are rhombohedral or "R-like", while the film on $LaAlO_3$ shows only the "T-like" phase. In contrast, the film on $YAlO_3$ shows a coexistence of both phases.

Figure 3. (color online) X-ray diffraction data for "T-like"-$BiFeO_3$ on $LaAlO_3$. **a**: RSMs in the pseudocubic [113] and [103] directions. **b**: In-plane diffraction θ-2θ scans through the substrate's 110_{pc} and 200_{pc} peaks.

Figure 4. (color online) Total calculated energy per formula unit of $BiFeO_3$ as a function of shear angle β. The optimized values of β are determined from a polynomial fit to each data set.

Figure 5. (color online) Strain and composition effects on the M_C phase. **a-b**: RSMs through the {226} and {206} peaks (i.e. in the $[113]_{pc}$ and $[103]_{pc}$ directions, respectively) for $BiFeO_3$ grown on $YAlO_3$. Approximate peak positions are indicated by crosses. **c-d**: Evolution of the lattice parameters as function of Ba-content in $Bi_{1-x}Ba_xFeO_3$ on $LaAlO_3$. Dashed lines are guides to the eye. **e-h**: RSMs through the {226} peaks for different values if x, and the {206} peaks for x = 0.08.

Figure 6. (color online) RSMs in the $[113]_{pc}$ (left column) and $[103]_{pc}$ (right) direction, for structures as indicated by the labels on the left. Effective stress increases from bottom to top. The path R-M_A -M_C-T corresponds to that indicated in Fig. 1a.

TABLE I. : Optimized structural parameters for competing phases *Cc*, *Pm* and *P1*.

	shear orientation	**β**	**a/b**	**tilt pattern**
***Cc* (M_A)**	[110]	88.1	1	$a^-b^-c^0$
***Pm* (M_C)**	[100]	90	1	$a^-b^0c^0$
P1	[100]	88.4	1.01	$a^-b^-c^0$

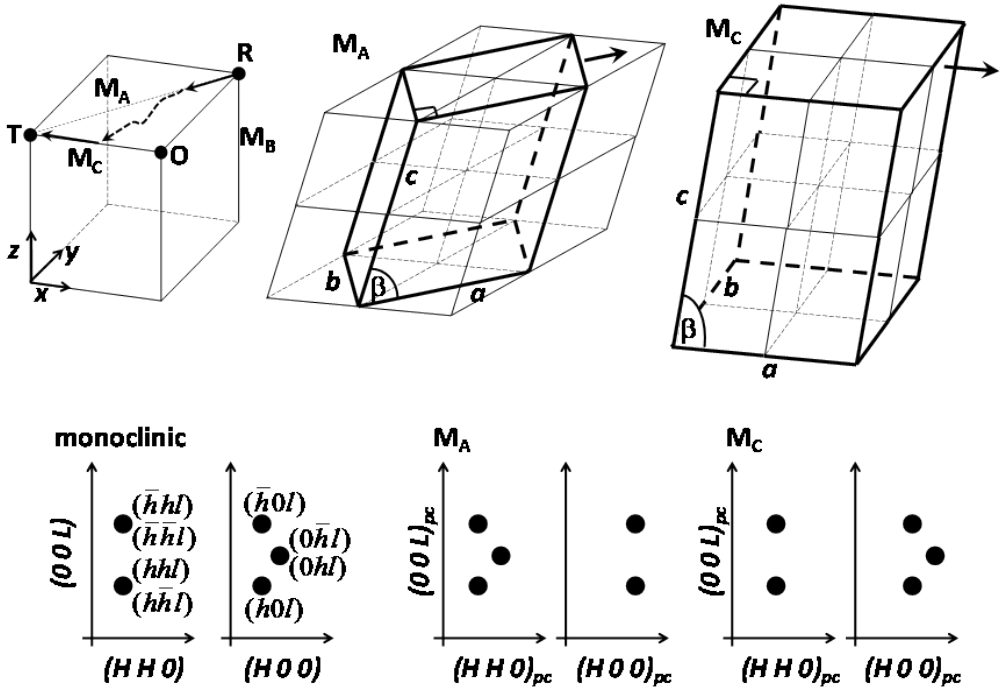

Figure 1. Schematic comparison of monoclinic structures. **a**: polarization direction in differently distorted perovskite structures: the polarization points in a direction parallel to that connecting the origin with the indicated dots for R, O, and T, or with any point on the lines labeled M_A, M_B, and M_C. The path R – M_A – M_C – T observed here and in relaxor ferroelectrics is indicated by arrows (see text). **b** and **c**: Smallest unit cells (with appropriate antiferromagnetic order and octahedral tilt patterns) for the two possible monoclinic structures, each resulting from a shear distortion in the direction of the indicated arrow. Thin lines indicate the primitive perovskite unit cell. M_A is a centered unit cell belonging to space group *Cc* or *Cm*, M_C is a primitive unit cell, space group *Pc* or *Pm*. **d**: Schematic representation of reciprocal space maps of a monoclinic structure, indexed in the monoclinic system and the pseudocubic notation for M_A and M_B, respectively.

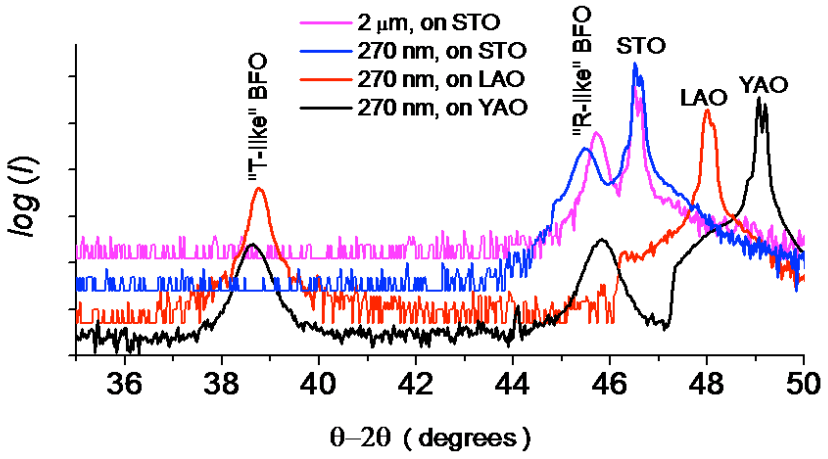

Figure 2. (color online) Comparison of $BiFeO_3$ (BFO) films grown on different substrates. The semi-logarithmic plot shows results from X-ray θ-2θ scans for four BFO films of different thickness and on different substrates (offset vertically for clarity): $SrTiO_3$ (STO), $LaAlO_3$ (LAO), and $YAlO_3$ (YAO). The 002_{pc} peaks for the film and substrates are shown. Films on $SrTiO_3$ are rhombohedral or "R-like", while the film on $LaAlO_3$ shows only the "T-like" phase. In contrast, the film on $YAlO_3$ shows a coexistence of both phases.

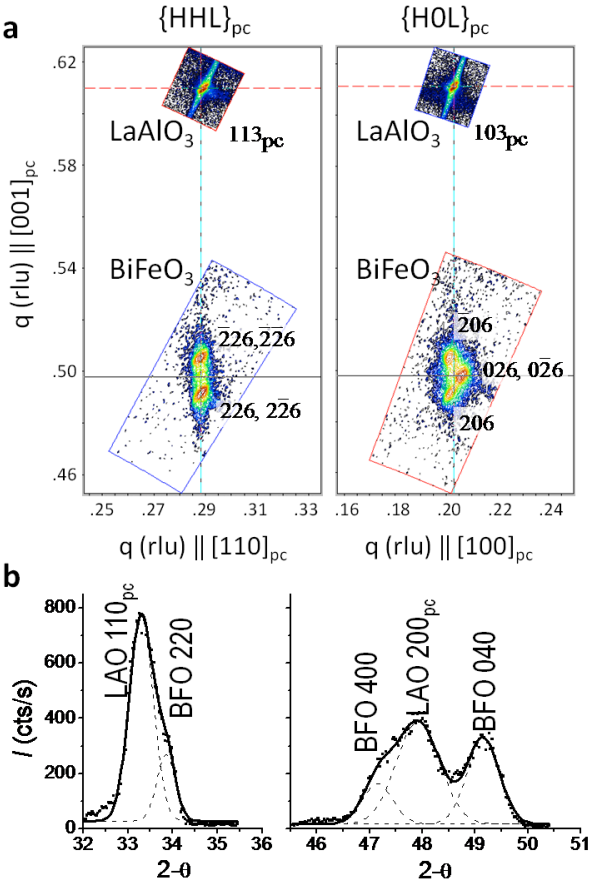

Figure 3. (color online) X-ray diffraction data for "T-like"-$BiFeO_3$ on $LaAlO_3$. **a**: RSMs in the pseudocubic [113] and [103] directions. **b**: In-plane diffraction θ-2θ scans through the substrate's 110_{pc} and 200_{pc} peaks.

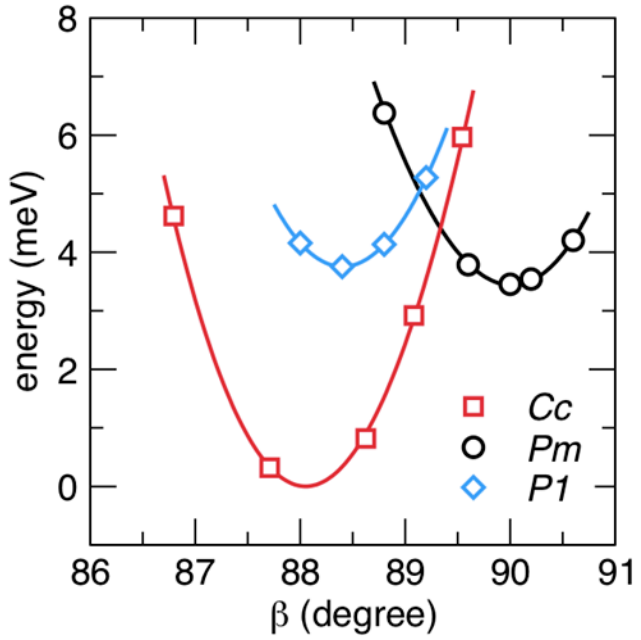

Figure 4. (color online) Total calculated energy per formula unit of $BiFeO_3$ as a function of shear angle β. The optimized values of β are determined from a polynomial fit to each data set.

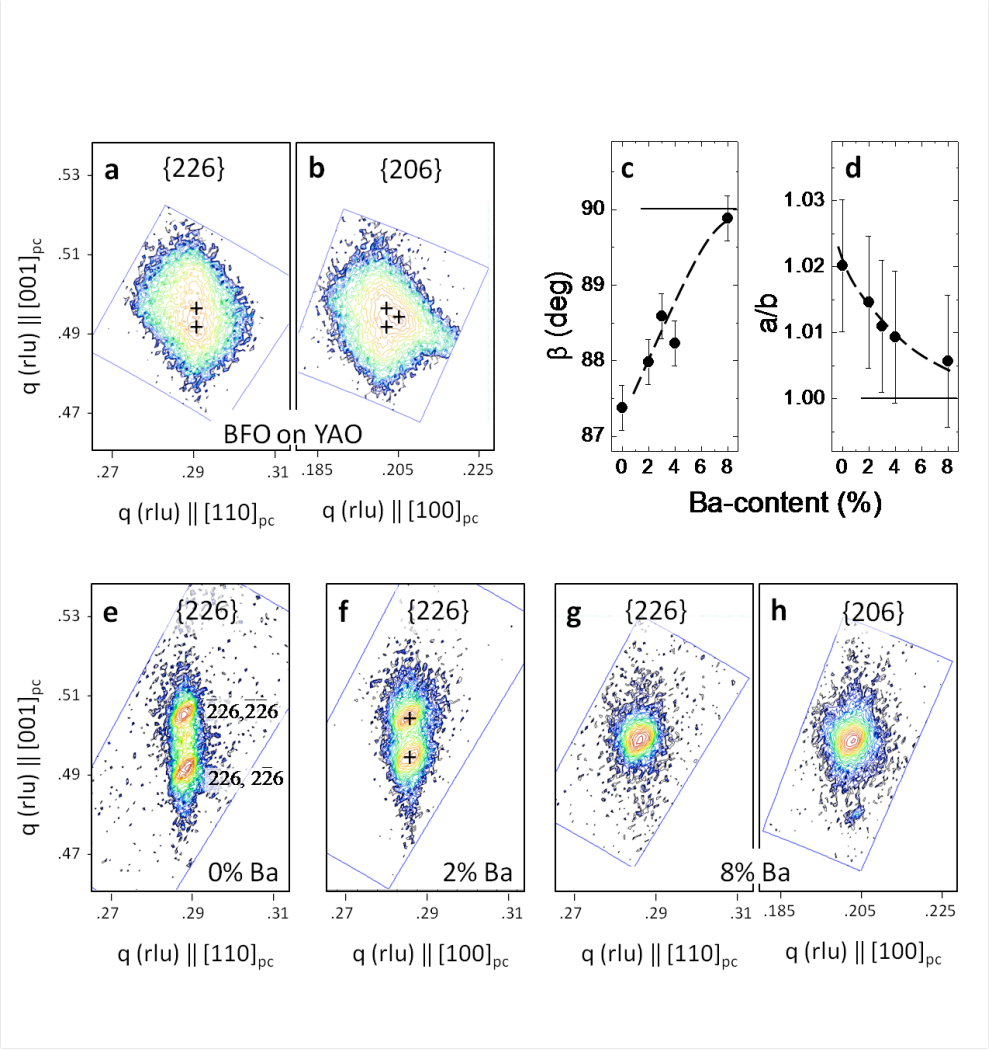

Figure 5. (color online) Strain and composition effects on the M_C phase. **a-b**: RSMs through the {226} and {206} peaks (i.e. in the $[113]_{pc}$ and $[103]_{pc}$ directions, respectively) for $BiFeO_3$ grown on $YAlO_3$. Approximate peak positions are indicated by crosses. **c-d**: Evolution of the lattice parameters as function of Ba-content in $Bi_{1-x}Ba_xFeO_3$ on $LaAlO_3$. Dashed lines are guides to the eye. **e-h**: RSMs through the {226} peaks for different values if x, and the {206} peaks for x = 0.08.

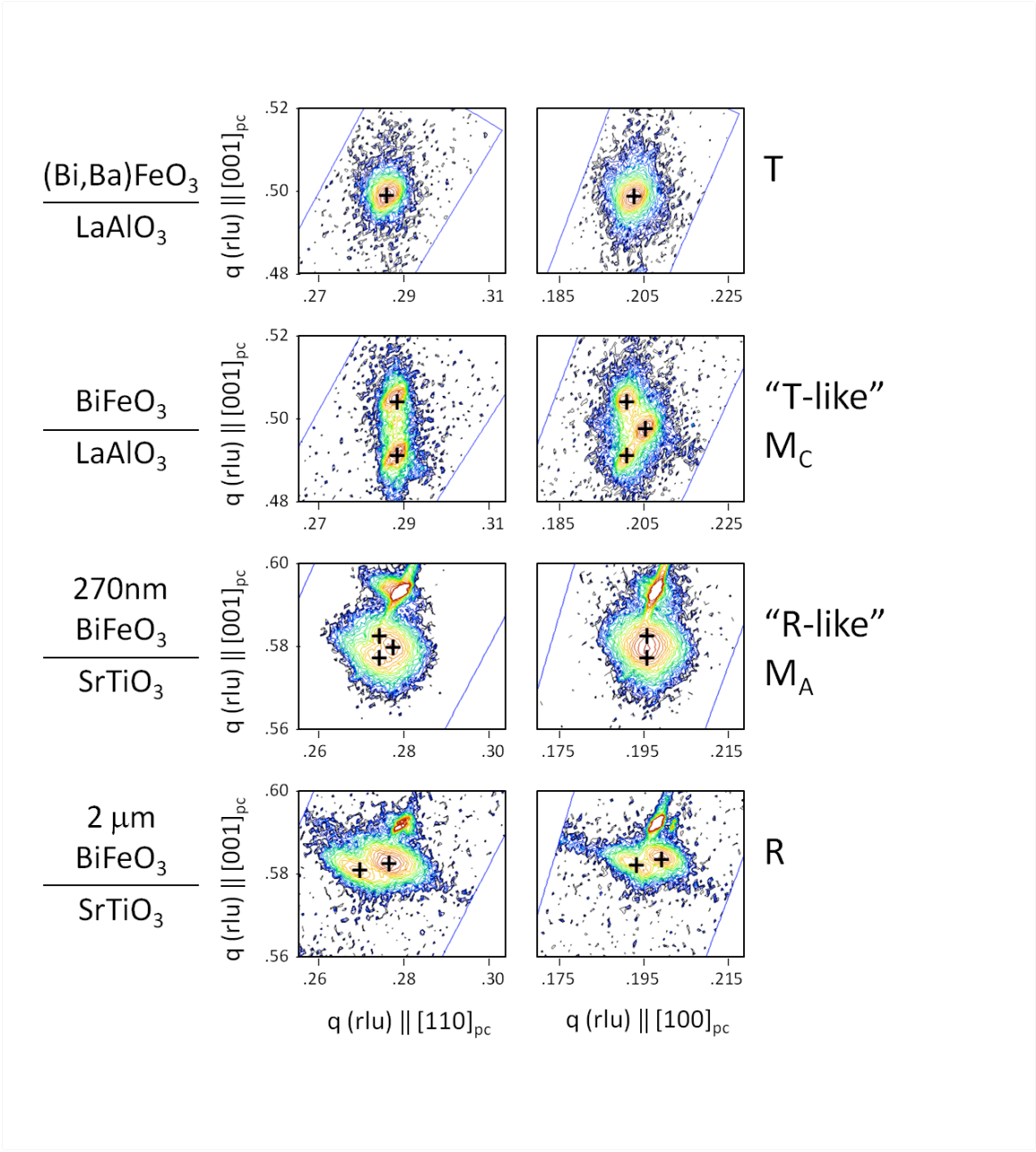

Figure 6. (color online) RSMs in the $[113]_{pc}$ (left column) and $[103]_{pc}$ (right) direction, for structures as indicated by the labels on the left. Effective stress increases from bottom to top. The path R-M_A -M_C-T corresponds to that indicated in Fig. 1a.